Indoor air quality analysis based on the ventilation effectiveness for CO_2 contaminant removal in ventilated cavities

J. Serrano-Arellano[a*], M. Gijón-Rivera[b], J.M. Riesco-Ávila[a], J. Xamán[c], and G. Álvarez[c]
[a]Departamento de Ingeniería Mecánica, Universidad de Guanajuato,
Carretera Salamanca-Valle de Santiago Km 3.5+1.8. Comunidad de Palo Blanco, Salamanca, Gto. C.P. 36885, México.
[b]Tecnológico de Monterrey Campus Puebla,
Vía Atlixcáyotl 2301, Reserva Territorial Atlixcayotl, Puebla, Puebla CP 72453, México.
[c]Centro Nacional de Investigación y Desarrollo Tecnológico, CENIDET-DGEST-SEP,
Prol. Av. Palmira S/N. Col. Palmira. Cuernavaca, Morelos C.P. 62490, México.

A theoretical study to determine an optimal configuration for removal a CO_2 contaminant from inside a room is presented. The geometry considered was a 2D ventilated cavity in turbulent flow regime and solving the governing equations of mass, momentum and chemical species by the finite volume method. The interval of Reynolds number under study was $0 \leq Re \leq 2.5 \times 10^4$. The air inlet gap is located on the lower side of vertical right wall of the cavity. Three configurations of the cavity varying the air outlet gap on vertical left wall were analysed: in the upper side (case A), in the middle side (case B), and in the lower side (case C). From the results, case A removed the most amount of contaminant from inside room for a $Re = 5 \times 10^3$, which had an effect on energy savings. The lower levels of contaminant for higher Reynolds numbers were obtained for the case B. The case C was the less desirable for contaminant removal purposes.

Keywords: Ventilation; indoor air quality; forced convection; turbulent flow; CO_2 contaminant.

PACS: 47.11.Df; 47.27.E-

1. Introduction

Ventilation process might be defined as the result of the intentional controlled introduction of outdoor air into occupied spaces through openings or gaps in the building envelope and it is the primary mechanism for removing contaminants from within buildings produced by people, equipment and materials. For natural ventilation systems, the outdoor air is driven towards the inside space due to temperature and pressure differences. The ventilation effectiveness depends on the size of inlets, air velocity, gaps locations, building orientation, etc. Natural ventilation is generally accompanied by mechanical ventilation, which allows a better control of whole-building ventilation requirements. Ventilation process is closely related to the comfort level experienced by a person. The comfort is a function of multiple variables such as: air temperature, radiant temperature, humidity, air velocity, type of clothing, activity levels, etc. It is well known that uncomfortable environments into buildings can lead to reduce the ability to concentrate and decrease motivation to work. On the other hand, unhealthy spaces may cause diseases produced by poor indoor air quality conditions [1]. The phenomenon mentioned above is called sick building syndrome and it is defined as a set of symptoms affecting occupants of buildings caused by the time spent in a building, but no specific illness or cause can be identified. These symptoms are: eyes, nose and throat irritation, headaches, colds, allergies, respiratory failures, among others. Human beings are the most important source of CO_2 inside buildings. Therefore, CO_2 as working fluid is very important in thermal and air quality design. The traditional way to model a ventilated

room is thorough cavities with different configurations and conditions. The ASHRAE norm [2] states the minimal requirements for having an acceptable air quality environment inside buildings and this work try to be suitable with standard guidelines.

From a literature review of ventilation systems and numerical applications, it was found some study for cavities as, [3] reported a numerical simulation of natural convection in rectangular cavities; the study was developed for porous and free medium. The formulation of the study was presented in terms of stream function and vorticity variable. Later, the authors [4] presented a numerical study of the natural convection in rectangular cavities by varying the aspect ratio. The parameters that influenced the evolution of the flow were the Rayleigh number and the aspect ratio. From the results it was found that the aspect ratio for different geometric values (G ≠ 1) flows in horizontal cavities, especially G < 1, flows are more active. Furthermore the maximum value find for Nusselt number was for an aspect ratio of G = 1/3.

Other several studies have been focused on building ventilation modeled as cavities, *e.g.*, [5] conducted a backward time modeling of diffusion-convection pollutant dispersions in a three-dimensional slot ventilated building. The authors investigated the effects of supplying inlet velocity, pollutant source location, diffusivity coefficient and pollutant releasing time. Results showed that the accuracy of recovering pollutant-releasing history reduces with the increasing inlet velocity, due to the thinner mass boundary layer forms with the enhanced forced convection [6]. Carried out a numerical study of laminar double-diffusive mixed convection in a ventilated cavity. The governing equations were solved by the

Galerkin finite element method. The authors varied the thermal Grashof numbers and results were presented in terms of streamlines, temperature and concentration distributions [7]. Investigated a three-dimensional flow in a cavity using large-eddy simulation (LES), the study included laminar and turbulent regimes ($Re = 3360$). The results showed for the laminar inflow, that the flow becomes unstable but remains laminar as it is convected over the cavity. For turbulent inflow, the fluctuation of the shear layer on top of the cavity by the incoming near-wall coherent structures strongly influences the formation and convection of eddies inside the separated shear layer [8]. Conducted a numerical simulation of heat and mass transfer in a ventilated cavity for nonstationary regimen and conductive walls. The intervals of the study were $Ra = 10^4 - 10^6$ and $Re = 200$. Results showed that thermal radiation decreases the optical thickness of the medium, and decreases the intensity of the heat exchange at the surface of the solid walls [9]. Performed a numerical procedure to evaluate the emergency ventilation of contaminant and occupants by using the efficiency factor of contaminant source to evaluate (EFCS). The authors examine the effects of source locations, ventilation modes and evacuation modes for optimal ventilation strategies. The results showed that the EFCS concept produce a reasonable way to evaluate the performance of emergency ventilation and that a system equipped with multiple ventilation modes was necessary since no universal ventilation mode can successfully mitigate all hazardous situations [10]. Conducted a numerical study of particles concentration in the air flow inside a room, for which they used three models of turbulence: the $k-\varepsilon$ model, the re-normalized $k-\varepsilon$ model (RNG) and the large eddy simulation (LES). The CFD computational model was solved by using the FLUENT program. The results were compared to those reported in literature. The authors concluded that the three models have a good agreement with experimental data, but the best result was obtained with the LES turbulence model [11]. Presented a 3-D numerical study to propose a uniform parameter: the integrated accessibility of contaminant source (IACS). This parameter combines the accessibility of contaminant source (ACS) and occupied density (OD) to protect indoor environment. From the results, it was observed that, displacement ventilation was more effective than mixing ventilation [12]. Performed a CFD study of a ventilated room to examine the characteristics of contaminated indoor air using the index of effectiveness of contaminant ventilation (IECV). The study analyzed different regions of inhalation for different positions of the human body and showed that the region of inhalation was greatly influenced by the rising stream of air resulting from the heat generated by metabolic activity [13]. Conducted a study of the influence of an occupied zone obstruction level, air distribution method, air change rate, cooling load and contaminant source. The results showed that the parameters mentioned above have small influence on the design of the air distribution system; the non-uniform distribution of the contaminant sources had the biggest influence

on the studied parameters. Recently, [14] conducted a numerical simulation to determinate the concentration distribution of CO_2 in a three dimensional model. The results showed that the concentration of CO_2 downwind decreased with increment of wind speed. Over a period of time, the concentration of carbon dioxide indoor kept constant. And vents or forced draft should be set to decrease the concentration of carbon dioxide [15]. Reported a numerical study for design of ventilation system to prevent the risk of spreading infections. The authors analyzed the influence of the positions of the air inlets. There were employed tree indices; quantify the capacity to renew the air, remove a contaminant and the risk of airborne infection. The results showed that the position of the air inlets and outlets has a great influence on the quality of the ventilation. The type of air diffuser has a notable influence on the air flow pattern and, therefore, on the likelihood of infection or any other ventilation quality index. Finally, the authors concluded that one type of diffuser cannot be extrapolated to other ones [16]. Reported a tracer gas method for a multi-zone test building to determinate the distribution of indoor air. The study focus two scenarios; how local heat sources can generate significant buoyancy driven flow and affect indoor mixing during wind-driven cross ventilation. A computational fluid dynamic (CFD) model was developed for the test building. The authors found that while the inlet temperature and overall ventilation rate seem to have little effect on air mixing generated by local buoyancy flow, the local heat flux was found to significantly impact the indoor air distribution [17]. Proposed a method to identify the quasi-steady indoor contaminant point source using some limited steady measured concentration data, the authors take an illustrative case, the identification was fulfilled successfully. But, when the measurement error is considered, the method needs to be improved for accuracy by increasing the number of the concentration measurement points (minimum 9 points when the concentration measurement error is 10%). [18] monitored a CO_2 concentration in a middle school to evaluate the indoor air quality and the ventilation rates in occupied classrooms. The results showed that the indoor CO_2 concentration exceeded the 1500 ppm value [19]. Performed an experimental and a numerical study to introduce a new index of air distribution. The index comprises parameters for assessing the indoor thermal comfort and air quality in occupied space. This index compared the performance of two ventilation systems (mixing ventilation and displacement ventilation). In general; the new index would be applicable to large spaces for evaluation the performance of a ventilation system.

According to the literature review, it was not found a ventilation study for CO_2 contaminant removal in a configuration as the proposed in the present study: three different contaminant sources locations on walls and turbulent flow regime. For this reason, this work aims to perform an analysis for CO_2 contaminant removal in a ventilated cavity in order to determine the best configuration for indoor air quality purposes.
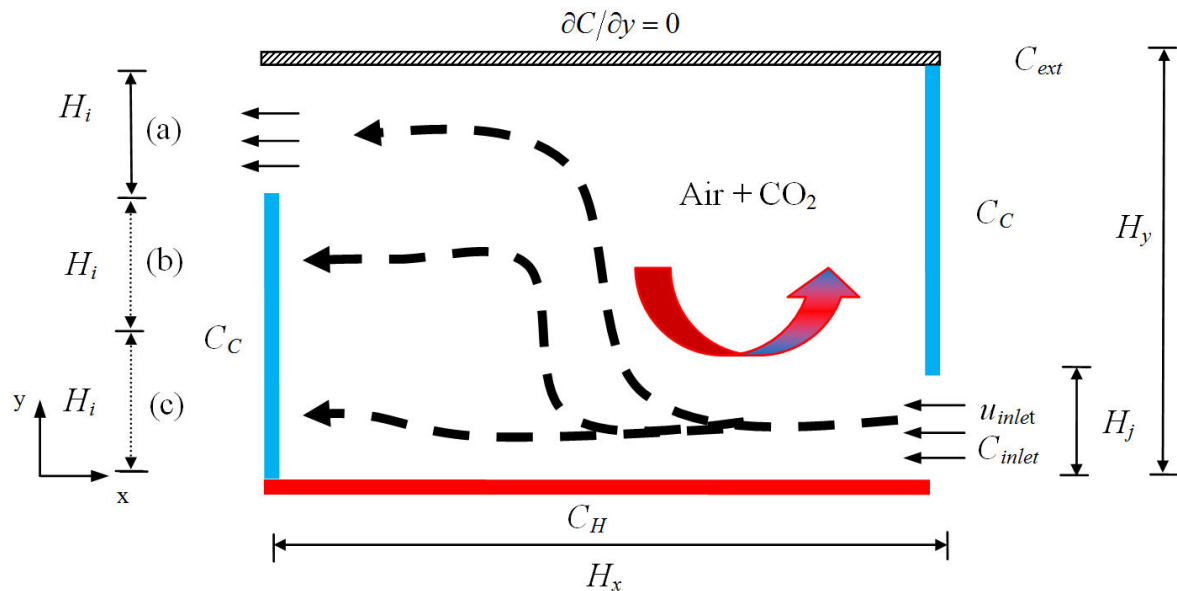
FIGURE 1. Physical model of the ventilated cavity under study.

2. Physical and mathematical model

The physical model consists of a two dimensional rectangular cavity of 4×3 m as shown in Fig. 1. The cavity is ventilated through the lower side of the vertical wall with air at a velocity $U_{\text{inlet}} = f(Re)$ and a CO$_2$ concentration $C_{\text{inlet}} = 360$ ppm. The inlet gap size is 0.3 m, which is the height considered in most air diffusers. The Air-CO$_2$ outlet gap is located in three different positions on the left wall: upper, middle and lower part of the wall. Vertical walls are considered with a lower contaminant concentration (C_C) of 1000 ppm and the horizontal bottom wall is set at a higher contaminant concentration (C_H) of 3000 ppm. The horizontal upper wall is assumed to be impermeable. Due to the CO$_2$ concentration differences among surfaces and the exterior surroundings, there is a concentration gradient producing the natural convection of the Air-CO$_2$ mixture inside the cavity. Induced movement by natural convection and the forced convection produced by the opening airflow gap circulate the mixture inside the cavity to the outlet gap of the cavity.

2.1. Convective mathematical model

The mathematical model formulation is established taking into account the following considerations: non-slip condition at walls is valid (zero velocity). The properties of the mixture of Air-CO$_2$ were assumed constant, except for the density in the buoyancy force term in the momentum equations, according to the Boussinesq approximation. The properties were evaluated at a reference concentration of $C_0 = (C_H + C_C)/2$. The working fluid is modeled as a Newtonian fluid in a turbulent regime. The mathematical model is expressed by the steady state governing equations of mass, momentum and chemical species in primitive variables of an incompressible fluid, as follows:

$$\frac{\partial(u_i)}{\partial x_i} = 0 \tag{1}$$

$$\frac{\partial(\rho u_i u_j)}{\partial x_j} = -\frac{\partial P}{\partial x_i}$$

$$+ \frac{\partial}{\partial x_j}\left[\mu\left(\frac{\partial u_i}{\partial x_j} + \mu\frac{\partial u_j}{\partial x_i}\right)\right]$$

$$- \overline{\rho u_i' u_j'} + \rho g_i \beta_c (C - C_\infty) \tag{2}$$

$$\frac{\partial(\rho \overline{u_j}\overline{C})}{\partial x_j} = \frac{\partial}{\partial x_j}\left(\rho D \frac{\partial \overline{C}}{\partial x_j} - \overline{\rho u_j' C'}\right) \tag{3}$$

where the Reynolds stress tensor $(\overline{\rho u_i' u_j'})$ and the turbulent mass flux vector $(\overline{\rho u_j' C'})$ can be approximated as:

$$\overline{\rho u_i' u_j'} = \mu_t\left[\frac{u_i}{\partial x_j} + \frac{\partial u_j}{\partial x_i}\right] + \frac{2}{3}\rho k \delta_{ij} \tag{4}$$

$$\overline{\rho u_j' C'} = -\frac{\mu_t}{Sc_t}\frac{\partial \overline{C}}{\partial x_i} \tag{5}$$

where Sc_t is the turbulent Schmidt number. The turbulent viscosity (μ_t) can be related with the turbulent kinetic energy (k) and the dissipation of turbulent kinetic energy (ε) through the Kolmogorov-Prandtl equation:

$$\mu_t = C_\mu \frac{\rho k^2}{\varepsilon} \tag{6}$$

where C_μ is a constant. The turbulent kinetic energy and the turbulent dissipation of kinetic energy can be obtained using its corresponding transport equations:

$$\frac{\partial(\rho u_i k)}{\partial x_i} = \frac{\partial}{\partial x_i}\left[\left(\mu + \frac{\mu_t}{\sigma_k}\right)\frac{\partial k}{\partial x_i}\right] + P_k + G_k - \rho\varepsilon \quad (7)$$

$$\frac{\partial(\rho u_i \varepsilon)}{\partial x_i} = \frac{\partial}{\partial x_i}\left[\left(\mu + \frac{\mu_t}{\sigma_\varepsilon}\right)\frac{\partial \varepsilon}{\partial x_i}\right]$$
$$+ C_{\varepsilon 1}[P_k + C_{\varepsilon 3}G_k]\frac{\varepsilon}{k} - C_{\varepsilon 2}\frac{\rho\varepsilon^2}{k} \quad (8)$$

where P_k and G_k are the sheer production of turbulence kinetic energy and the buoyant production/destruction of turbulence kinetic energy respectively. The $k-\varepsilon$ turbulence model defines the following variables $C_{\varepsilon 1} = 1.44$, $C_{\varepsilon 2} = 1.92$, $C_{\varepsilon 3} = \tan h|v/u|$, $C_\mu = 0.09$, $\sigma_k = 1.0$ and $\sigma_\varepsilon = 1.3$. After defining the governing equations are established boundary conditions of the mathematical convective model. The mathematical boundary conditions for the fluid domain are as follow: velocity components on solid surfaces are zero ($u = v = 0$). The velocities at the air inlet gap are $u = u_{\text{inlet}}$ y $v_{\text{inlet}} = 0$ and at the mixture outlet gap $\partial u/\partial n = 0$ and $\partial v/\partial n = 0$, where n is the normal vector in the flow direction.

Boundary conditions for the chemical specie (CO_2) are $C = C_{\text{inlet}}$ and at the mixture outlet gaps we have $(\partial C/\partial n)$=0. For boundaries interacting with the cavity, the contaminant concentration is assumed to be constant at C_H o C_C, except on horizontal upper wall where the surface is considered impermeable. Boundary conditions for the turbulent transport ($k - \varepsilon$) are $k = 1.5(0.04u_{\text{int}})^{2.0}$ and $\varepsilon_{\text{int}} = (k_{\text{int}})^{0.5}/(0.1H_i)$ at the air inlet gap and at the air outlet gap are: $(\partial k/\partial n)$=0 y $(\partial \varepsilon/\partial n)$=0. All solid surfaces are subject to constant values of and as proposed by [20].

2.2. Overall ventilation effectiveness for contaminant distribution ε_C

The overall ventilation effectiveness for contaminant distribution $\bar{\varepsilon}_C$ provides a quantitative index related to the way in which contaminant is distributed all over inside the cavity [21]. Defined this parameter as function of the following variables:

$$\bar{\varepsilon}_C = \frac{C_{\text{outlet}} - C_{\text{inlet}}}{C_{\text{average}} - C_{\text{inlet}}} \quad (9)$$

where, C_{outlet} is the average contaminant concentration of the mixture of Air- CO_2 at the air outlet gap and C_{average} is the average contaminant concentration of the mixture inside the cavity. Finally, C_{outlet} is the average contaminant concentration of the mixture at the air inlet gap.

3. Numerical Procedure

The governing equations described above are numerically solved using the finite volume method developed by [22]. The velocity components are calculated at a staggered grid while the scalar variables are calculated at the main grid (not staggered). In order to implement the numerical algorithm, the governing equations can be represented by the following general equation of convection-diffusion:

$$\frac{\partial}{\partial x_j}(\rho u_j \phi) = \frac{\partial}{\partial x_j}\left(\Gamma\frac{\partial \phi}{\partial x_j}\right) + S_\phi \quad (10)$$

The integration of Eq. (10) over the corresponding finite volume and substitution of every term by discrete values of ϕ in the nodal points gives the following algebraic equation for every nodal point:

$$a_p\phi_p^{n+1} = \sum_{nb} a_{nb}\phi_n b^{n+1} + S_\phi \Delta V + \rho^n \Delta V \phi_p^n \quad (11)$$

where n y nb represent the number of iterations and the coefficients for neighbouring nodes respectively. The convective terms are formulated by the power law scheme and diffusive terms by the central scheme. The coupling between momentum and continuity equations is made with the SIMPLEC algorithm proposed by [23]. The algebraic equations systems obtained with Eq. (11) are solved applying the line by line method (LBL) with alternating direction implicit scheme (ADI). Moreover, under-relaxation is introduced using the false transient strategy to improve the convergence. The global convergence reflected in mass balance that applies to all control volumes. If the values in the mass balance for every control volume as well as the residual values of the different equations are sufficiently low, overall convergence is obtained (typically 10^{-8}). The above convergence criterion assures an acceptable solution. The general procedure for the numerical simulation can be summarized in the following steps: (1) initial values are assumed for all variables (u, v, P, $C\ldots\varepsilon$). (2) The velocity-pressure (u, v, P) were calculated by the SIMPLEC algorithm. (3) With the new calculated values of velocity, the CO_2 concentration (C), the turbulent kinetic energy (k) and the dissipation of turbulent kinetic energy (ε) were obtained. A convergence criterion was applied and the process was repeated iteratively until the convergence was achieved. The accuracy of the numerical results was verified through a grid independence study. The mesh independence study was carried out varying from 91×61 to 121×111 with 10 nodes increments on each axis. It was found an adequate mesh for 111×101 used in all cases considered because a maximum deviation of 1% for the variables between meshes 111×101 and 121×111 was observed.

3.1. Validation and verification of numerical code

In order to validate the developed numerical code, the ventilated cavity under isothermal conditions and turbulent flow regime reported by [24] was solved. The verification and validation processes were presented by [25], with satisfactory results. Furthermore, the verification process was completed considering the problem published by [26] to perform a quantitative numerical comparison between solutions. The problem consists on a 2D rectangular cavity with several inlet/outlet configurations and different contaminant source locations in laminar and turbulent flow regimes. The particular case of the top-top (TT) configuration in steady state was
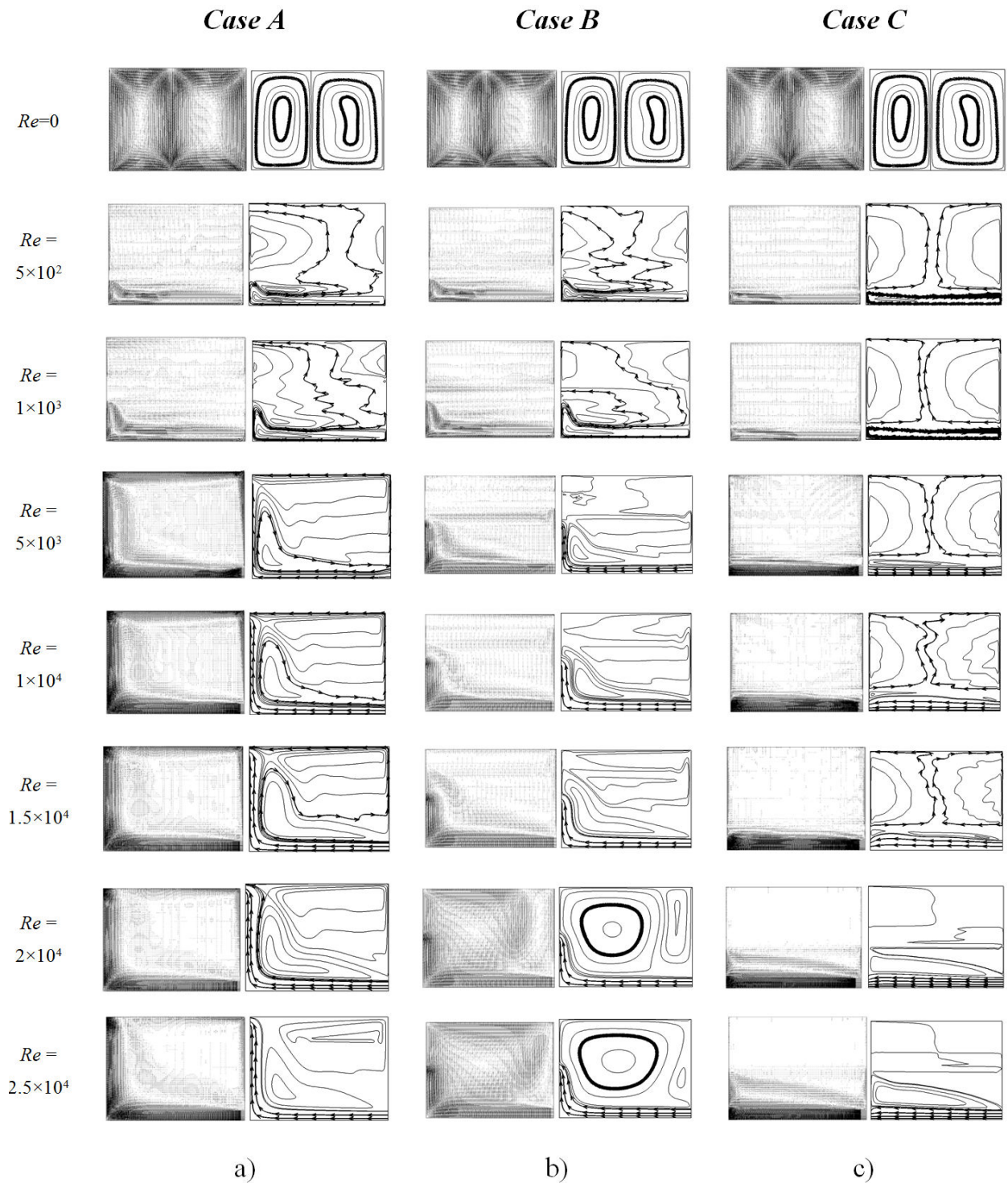
FIGURE 2. Vector field and streamlines as a function of the Reynolds number in the ventilated the cavity.

compared with the present study and results are shown in Table I. It can be appreciated that the final average concentration value for the case C had a maximum deviation of 1.4% which indicates that the numerical code developed for this study, shows satisfactory results.

4. Results and discussions

Calculation results of the ventilated cavity with a mixture of Air-CO_2 are graphically presented in Figs. 2 and 3. The varying parameters for this study are: (1) the inlet fluid velocity (u_{inlet}), which varied from 0 (closed cavity), 0.03, 0.05, 0.26,

TABLE I. Quantitative verification of the average CO_2 concentration with different contaminant sources locations inside the cavity.

Contaminant Source Location	Lage and Bejan [26]	Present Study	Differences %
Case A	75.26	74.6	0.87
Case B	55.51	56.2	1.22
Case C	47.91	47.2	**1.4**
Case D	122.24	121.8	0.3
Case E	73.16	73.2	0.05

0.52, 0.78, 1.04, 1.30 m/s, and their corresponding Reynolds number are 0 (closed cavity), 5×10^2 1×10^3, 5×10^3, 1×10^4, 1.5×10^4, 2×10^4, and 2.5×10^4 respectively; (2) location for the fluid outlet in the cavity, for this parameter three configurations were considered: Case A (outlet aperture on the upper side of the left wall), Case B (outlet aperture on the middle side of the left wall) and Case C (outlet aperture on the bottom side of the left wall).

4.1. Flow pattern results

Vector field, streamlines, masslines and isoconcentration for different values of Re are shown next; all configurations were considered with a lower concentration of 1000 ppm (C_C) on vertical walls and a higher concentration of 3000 ppm on the horizontal bottom wall.

The vector field and streamlines within the interval under study are shown in Fig. 2. In general, it can be observed that flow distribution of the Air-CO_2 mixture for $Re = 0$ are generated by buoyancy forces producing concentration gradients. In this situation the flow pattern inside the cavity forms two parallel vortexes vertically extended due to the natural convection generated by the impulse from the high concentration bottom wall towards each lower concentration vertical wall. When natural convection prevails, the flow pattern is divided into two symmetrical recirculation zones as an ideally closed cavity. Instead, for Re values of 5×10^2 and 1×10^3 it can be clearly observed how forced convection starts to be relevant due to the inlet flow supplied through the gap aperture which produces flow distortions inside the cavity. The resulting flow patterns for cases A and B are very similar for both Re numbers with a recirculation at the lower side of the cavity and irregular flow at the rest of the indoor space. For configuration C, the flow pattern generates two symmetrical recirculations at the upper side of the cavity and one more elongated vortex close to the bottom part of the enclosure.

From an interval of $5 \times 10^3 \leq Re \leq 1.5 \times 10^4$, cases A and B change their flow pattern by non-uniform recirculations with a highly stratification of the fluid at the upper side of the cavity and a dominant extended recirculation driven from bottom wall and rises close to the left wall until reaching the outlet aperture. The case C has not important changes with respect to cases for lower Reynolds numbers; this be-

havior can be mainly explained because the flow entering and leaving the cavity does not cause a significant alteration on the stratified fluid at almost the whole space of the cavity.

For a $Re = 2 \times 10^4$, the flow pattern for configuration B has considerably changed with a main circular vortex arises at the upper side of the cavity. In the case C, the two parallel recirculations presented above tend to disappear and the fluid flows towards the air outlet gap without any important recirculation. Finally, for $Re = 2.5 \times 10^4$ it can be seen how case A has a tendency to reduce the recirculation at the upper zone of the cavity, whereas cases B and C maintain a similar behavior with regard to previous Reynolds numbers.

It can be note that the masslines for all Reynolds numbers have a qualitative similar behavior than streamlines and they are shown in Fig. 3. For natural convection ($Re = 0$), the mixture of Air-CO_2 is shaped by two recirculations indicating their opposite direction of the mass flow. For a $Re = 5 \times 10^2$ and $Re = 1 \times 10^3$ a distorted flow is formed with a lower intensity located at the left upper corner side of the cavity for the three cases of study. When $Re = 5 \times 10^3$ the intensity of mass flow tend to be more uniform and maintain the fluid movement in a single clockwise direction. Also it is noticeable that for case C and $Re = 2.5 \times 10^4$, the mass flow intensity is completely uniform with values of 180 in magnitude. In general, it can be observed that the direction of mass flow is defined by the forced convection as well as concluding that the intensity contributes to have a more uniform flow. On the contrary, if the natural convection is presented, the mass flow generates recirculations in opposite directions with different flow intensities in several zones inside the cavity.

The Fig. 3 shows the behavior of isoconcentrations at the inside of the cavity. It can be observed that for a $Re = 0$, symmetrical recirculations are presented at two zones of the cavity with maximum levels of contaminant concentration due to the natural convection dominating the flow pattern. In this regard, the CO_2 concentration levels are mostly uniform through the cavity and within the interval of 1958-1966 ppm.

When a forced flow is induced by the inlet aperture (inlet air velocity starts to be important), the isoconcentration patterns are quasi parallel in horizontal direction in most of the cavity space for the three cases of study with slightly perturbations near the horizontal bottom wall. The flow pattern is still driven by diffusion with lowest concentration values closed to the lower horizontal wall, which is the zone where the mixture of clean air and lowest CO_2 concentration are present. For $Re = 5 \times 10^3$, the lowest concentration levels are presented for case A, with values lower than 514 ppm.

When increasing the Reynolds number ($5 \times 10^3 \leq Re \leq 2 \times 10^4$), the isoconcentration tend to generate a "L" shaped main vortex closed to vertical left wall and towards the air outlet gap for case A. Also, it can be seen how for $Re = 5 \times 10^3$ the level of concentration has considerably decreased regarding cases B and C, where the higher concentration levels are located at the upper side of the cavity. From a $Re = 1 \times 10^4$, the case B shows the lower contaminant
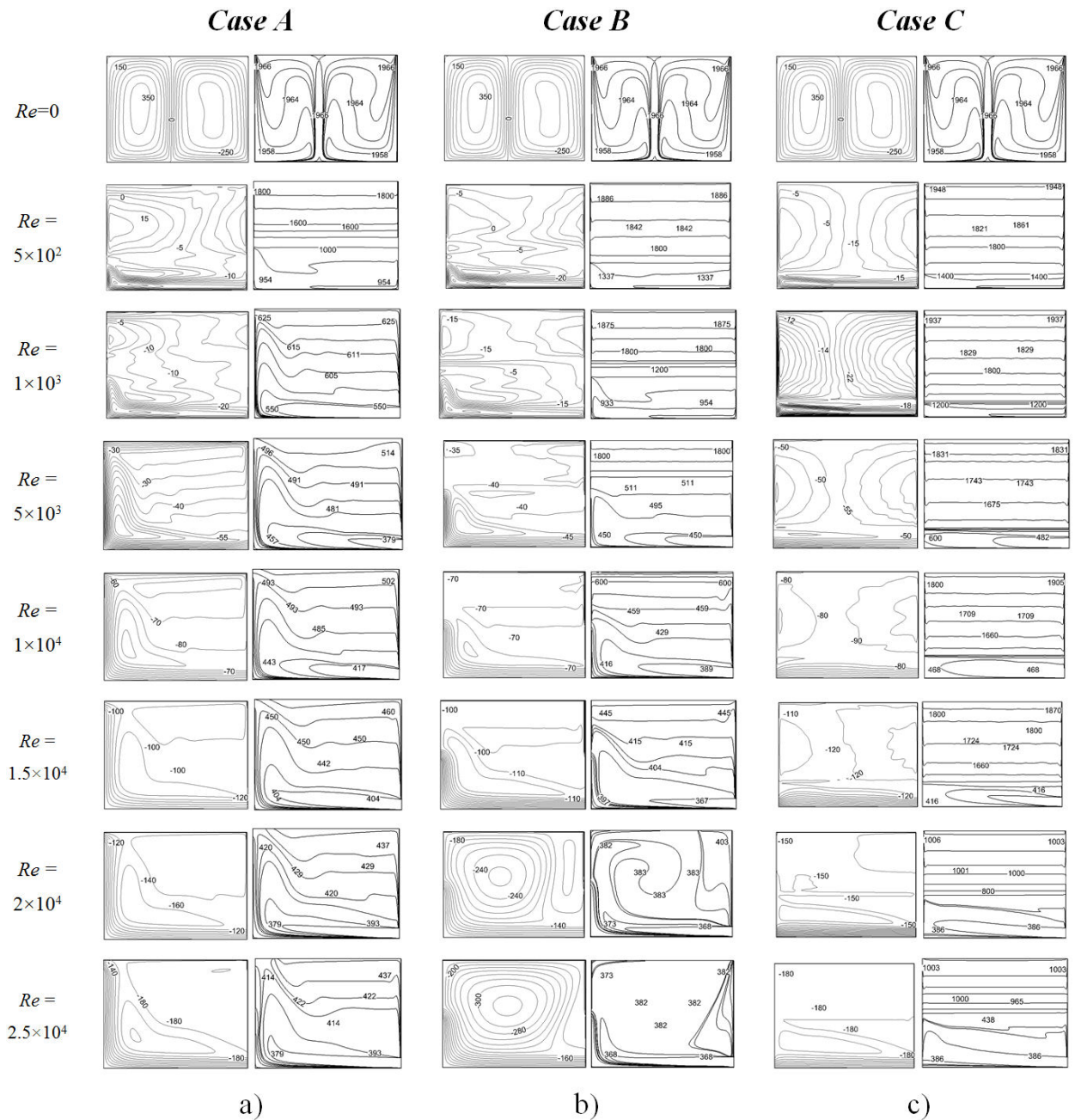
FIGURE 3. Masslines and isoconcentration (ppm) as a function of the Reynolds number in the ventilated the cavity.

CO$_2$ concentration among cases; for instance, at the same inlet airflow velocity ($Re = 1 \times 10^4$) a concentration reduction of approximately three times lower than previous Reynolds number at the upper side of the cavity is presented. On the contrary, the case C continues with higher concentrations at the upper zone of the cavity ($\sim$ 1800 ppm). From a qualitative comparison between $Re = 1.5 \times 10^4$ and $Re = 2 \times 10^4$, it can be seen how the case A maintains a similar concentration pattern, whereas the case B have substantial differences.

Finally, for $Re = 2.5 \times 10^4$, the lower concentration level for all Re numbers analyzed is presented. However, the case

A does not show a significant decrease of concentration levels compared to the previous Reynolds number ($\sim$ 6 ppm). While the case B presents an average reduction of 1 ppm at the center of the cavity. On the other hand, the case C shows two zones divided by lower and higher concentrations values producing the worst air quality conditions among cases.

4.2. Average CO$_2$ concentrations inside the cavity

In order to quantitatively compare configurations regarding to the highest values of $\bar{\varepsilon}_C$, Table II shows the corresponding average concentration values of CO$_2$ (C_{average}) for configura-

TABLE II. Average CO_2 concentration inside the cavity (ppm).

Re	0	5×10^2	1×10^3	5×10^3	1×10^4	1.5×10^4	2×10^4	2.5×10^4
				C_{average}				
Case A	**1962**	1666	1335	**597**	**481**	443	423	415
Case B	**1962**	1683	1399	830	**482**	416	386	**381**
Case C	**1962**	1768	1712	1525	**1469**	1442	753	696

tions A, B and C as a function of Re. In this table, it can be observed that higher concentrations are presented for for $Re = 0$, which is explained due to the fluid movement induced by pure diffusion. It is important to note that from $Re > 1 \times 10^4$, the CO_2 concentration decreases only by approximately 10%. Furthermore, the case C presents an important reduction of 50% of concentration levels until a $Re = 2.0 \times 10^4$ was reached. Ultimately, for a $Re = 2.5 \times 10^4$, the case B shows the lowest pollutant concentration with a value 381 ppm throughout the interval under study.

4.3. Overall ventilation effectiveness for the removal of pollutants ε_C

The pollutant removal effectiveness ε_C, provides a quantitative index related to the way in which pollutants are distributed all over inside the cavity, the higher value the more homogeneous pollutants distribution. This air quality parameter is very important in building design because the contaminant can be stratified in particular zones with high levels of pollutants and it can be difficult to observe the whole Air-CO_2 distribution by taking into account only average concentration values. Figure 4 shows the results for ε_C, for all the configurations considered in this work. It can be seen from figure that for the case A, the CO_2 contaminant distribution reaches a maximum value for $Re = 1 \times 10^3$ and later it is

FIGURE 4. Overall ventilation effectiveness for the removal of pollutants as function of Reynolds number for all cases.

kept approximately constant. Regarding case B, it was found a minimum ε_C value for $Re = 5 \times 10^3$, owing to high concentration gradients presented at the upper and lower side of the cavity. Moreover, the maximum contaminant distribution efficiency among cases is reached for $Re = 2 \times 10^4$ and 2.5×10^4. Lastly, the case C presents the maximum value of ε_C when natural convection is predominant ($Re \leq 1 \times 10^3$). This behavior indicates the need to supply air at higher velocities as possible in order to improve the interaction between clean air inlet and the CO_2 contaminant existing inside the cavity.

5. Conclusions

A numerical study of a two dimensional ventilated cavity for indoor air quality design was presented. From the results, it can be concluded that:

- From the flow pattern distribution, it was qualitatively observed that for natural convection cases ($Re = 0$), two symmetrical recirculation cells were formed close to vertical walls dividing the cavity in two zones with opposite flow direction with each other.

- Once the air inlet velocity increased the forced flow start to be dominant over free flow. For the case A, the level of contaminant concentration rapidly decreased until $Re = 5 \times 10^3$. From here, the pollutant reduction by increasing the air inlet velocity was turned to be less relevant: 20, 8, 4 and 2%, from $Re = 1 \times 10^4$ up to $Re = 2.5 \times 10^4$, progressively. As a conclusion, the case A was the best configuration in order to maintain acceptable contaminant concentration levels with low electric energy consumption for end users.

- It was found that the case B reached lower contaminant levels from $Re = 2 \times 10^4$ with a maximum reduction of 35% compared with case A. However, due to the higher air inlet velocities supplied (four times that case A), the electricity cost and environmental impact were higher. Therefore, the configuration B is recommended only if higher air quality requirements are mandatory.

- The configuration C was the worst configuration for contaminant removal purposes even for higher air inlet velocities ($Re \geq 2 \times 10^4$). From the results, it was shown that the cavity is divides by two zones: the high
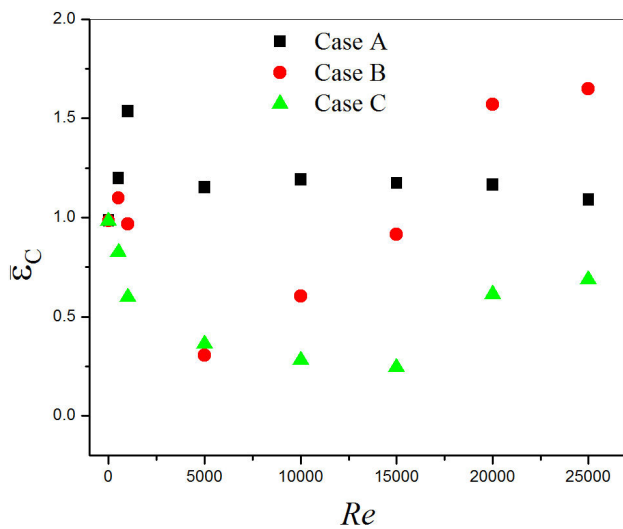
CO$_2$ concentration (~ 1000 ppm) at the upper side and the low CO$_2$ concentration (~ 400 ppm) at the lower side of the cavity.

- Case A reached the maximum value for ventilation effectiveness index with $Re = 1 \times 10^3$, after this value begins to decline. For the other cases the maximum value for ventilation effectiveness index was reached with high Re values.

- From an air quality point of view, the Standard ASHRAE 62-2007 [2] states that the maximum con-

centration of carbon dioxide (CO$_2$) inside a room environment is 700 ppm. In order to be acceptable for air quality purposes, the case A fulfills this requirement with a Reynolds of 5×10^3. However, if it requires high cleanliness in the room, the case B achieves the best air quality with a Reynolds value of 2.5×10^4.

Acknowledgments

1. M.M. Monroy, *Calidad ambiental en la edificación* (Manuales ambientales CARO, 2005). pp. 113-125.

2. ASHRAE Standard 62-2007, Ventilation for acceptable indoor air quality.

3. E. Baez, B. Bermúdez, and A. Nicholas, *Rev. Mex. Fis.* **50** (2004) 36.

4. B. Bermudez and A. Nicolas, *Rev. Mex. Fis*. **54** (2008) 236.

5. Di Liu, Fu-Yun Zhao, Han-Qing Wang, and Ernst Rank, *Int. J. Thermal Sciences* **64** (2013) 81.

6. Sumon Saha, Mohammad Nasim Hasan, and Iftheker Ahmed Khan, *Chem. Eng. Res. Bull.* **13** (2009) 17.

7. Kyoungsik Chang, George Constantinescu, and Seung-o Park, *J. Fluid Mech.* **561** (2006) 113.

8. M. A. Sheremet and N. I. Shishkin, *J. Eng. Phys. Thermophys.* **85** (2012) 828.

9. Hao Cai, Weiding Long, Xianting Li, and Douglas Barker, *Build. Environ.* **45** (2010) 485.

10. Z.F. Tian, J.Y. Tu, G.H. Yeoh, and R.K.K. Yuen, *Build. Environ.* **41** (2006) 1504.

11. Bin Zhaoa, Xianting Li, Xi Chen, and Dongtao Huang, *Build. Environ.* **39** (2004) 1035.

12. Tatsuya Hayashi, Yoshiaki Ishizu, Shinsuke Kato, and Shuzo Murakami, *Build. Environ.* **37** (2002) 219.

13. K. Hagstrom, A.M. Zhivov, K. Sirén, and L.L. Christianson, *Build. Environ*. **37** (2002) 55.

14. Zhirong Wang, Yuanyuan Hu, and Juncheng Jiang, *Energy Build*. **66** (2013) 461.

15. J. M. Villafruela, F. Castro, J. Francisco San José, and J. Saint-Martin, *Energy Build*. **57** (2013) 210.

16. L. James Lo and Atila Novoselac, *Build. Simul.* **6** (2013) 69.

17. Xinke Wang, Wei Tao, Yuanyuan Lu, and Fenghao Wang, *Build. Simul.* **6** (2013) 395.

18. Cristina Cornaro, Alessandro Paravicini, and Annamaria Cimini, *Indoor Build. Environ.* **22** (2013) 445.

19. I. Almesri, H.B. Awbi, E. Foda, and K. Sirén, *Indoor Build. Environ.* **22** (2013) 618.

20. R. Henkes, F. Van-Der-Vlugt, and C. Hoogendoorn, *Int. J. Heat Mass Tran.* **34** (1991) 377.

21. H. Awbi, *Ventilation of Building*, (E & FN Spon, 2003), pp 80-82.

22. S. Patankar, *Numerical heat transfer and fluid flow*, (Hemisphere Publishing Co., Mc. Graw Hill Co., New York, 1980), pp.113-135.

23. J. Van Doormaal and G. Raithby, *Num. Heat Tran*. **7** (1984) 147.

24. P. Nielsen, *Energy Cons. Build. Comm. Sys. An*. 20, Denmark, Nov., (1990).

25. J. Serrano-Arellano, J. Xamán, and G. Álvarez, *Int. J. Heat Mass Tran.* **62** (2013) 9.

26. J. Lage and A. Bejan, *Int. J. Heat Mass Tran.* **35** (1992) 1169.